Al-Si@Al(OH)3 Nanosheets Composite for Enhanced Efficient Strategy to Synthesize Al-Si@Al2O3 Core-shell Structure

Yuhui Lin
Qingdao University of Science and Technology
Panyu Chen
Qingdao University of Science and Technology
Ying Wang
Qingdao University of Science and Technology
Wei He
State Grid Electric Power Research Institute
Chao Tang
State Grid Electric Power Research Institute
Limin Wang
State Grid Electric Power Research Institute
Chengdong Li (2538163190@qq.com)
Qingdao University of Science and Technology

Research Article

Keywords: Surfaces, Nanocomposite, Microstructure, Al-Si particles, Al(OH)3 nanosheets

Posted Date: June 18th, 2021

DOI: https://doi.org/10.21203/rs.3.rs-604985/v1

Abstract

Owing to the combined advantages of Al-Si alloy and Al_2O_3, Al-Si@Al_2O_3 is widely utilized as a heat storage material, catalyst carrier and what adsorption host. Hence, the preparation of Al-Si@Al_2O_3 and corresponding precursors is of utmost significance. Herein, Al-Si@$Al(OH)_3$ precursor is investigated and $Al(OH)_3$ nanosheets are in-situ formed on the surface of Al-*x*Si alloy (*x* = 10, 20 and 30) in the presence of water. The influence of Si content, diameter of Al-Si particles and heating parameters on morphology and thickness of $Al(OH)_3$ nanosheets is systematically explored using X-ray diffraction, electron microscopy, Fourier transform infrared spectroscopy and N_2 adsorption/desorption isotherms. The growth mechanism of $Al(OH)_3$ nanosheets is revealed and a pathway to obtain Al-Si@Al_2O_3 nanosheets with desired structure and thickness is demonstrated.

Introduction

The term core-shell structure first appeared in nanotechnology and extended to various subject areas. The core-shell structure is a two-component system that combines both components' respective characteristics to meet the intensive requirements of the advanced applications [1]. Recently, core-shell structured materials have garnered significant research attention due to their comprehensive properties and designability as photocatalysts [2], thermal storage material [3], and adsorption material [4]. Different methods can be used to obtain the core-shell structures, including hydrothermal method [5–7], sol-gel process [8–10], arc discharge method [11–13] and one pot approach [14–16].

The Al-Si alloy is a cost-effective, highly conductive and thermally stable candidate, which can easily form a core-shell structure with Al-Si particle as a core and Al_2O_3 as a shell [17]. The low specific area and high-temperature corrosion of Al-Si particles, however, greatly limit the practical applications. Hence, alumina (Al_2O_3) is usually coated on the surface of Al-Si particles due to its high specific area, chemical inertness and thermal stability [18]. For instance, Han et al. [19] have reported a facile hydrothermal process to synthesize γ-Al_2O_3 on the surface of Al-40Si powder, revealing the growth mechanism of AlOOH nano-flakes on the surface. Dai et al. [20] have prepared Al-Si@Al_2O_3 by hydrothermal method and further investigated the effect of size and aluminum content in Al-Si powder on the catalytic performance of Pb/Al-Si@Al_2O_3. The results indicated that Pb/Al-Si@Al_2O_3 catalyst possessed optimal hydrogenation performance when the size and aluminum content were 5 μm and 88%, respectively.

Al-Si powder, with different amounts of Si, exhibits different morphologies [21–23]. The eutectic Si can be observed when Si content in Al-Si powder is less than 12.6 at. %. In contrast, eutectic Si and primary eutectic coexist in Al-Si powder when Si content is higher than 12.6 at. %. Meanwhile, primary Si became more irregular and larger with the increase of Si content. These studies demonstrate that AlOOH nucleates at Si substrate, however, the influence of Si morphology on nucleation of hydrated alumina has been neglected in these studies.

Herein, Al-Si powder, with different amounts of Si, is selected to explore the impact of Si morphology to $Al(OH)_3$ nucleation. Research showed that the morphology can be maintained while the phase change was arose from boehmite to γ-Al_2O_3 [4]. Hence, instead of calcination temperature, the structure of Al_2O_3 is mainly influenced by the Si content. Silicon morphology of Al-Si powders has different characteristic in diverse particle size which is resulted from solidification rate [24], the particle size is also a significant research factor. Furthermore, $Al(OH)_3$ was prepared on the surface of Al-Si particles using the hydrothermal and water bath methods. In addition, the influence of reaction time, Si content and particle size on the structure of Al-Si@$Al(OH)_3$ precursor is discussed, and the mechanism of in-situ formation of $Al(OH)_3$ nano-flakes is investigated.

Experimental

Al-Si powder was treated using deionized water at 80 ℃ for 3 h under the hydrothermal method, followed by centrifugation, washing with absolute alcohol thrice and drying at 50 ℃ for 12 h. This process resulted in Al-Si@$Al(OH)_3$ sample. Moreover, Al-Si@$Al(OH)_3$ sample was prepared using the water bath method under the same conditions. With different amounts of Si and particle sizes, Al-Si powder was utilized to obtain different samples, as detailed in Table 1. The Al-Si powder, with 12 at. % of Si and a diameter of 75 μm, was labeled as A17. The A17 sample was hydrothermally treated for 3 h to synthesize Al-12Si@$Al(OH)_3$ and the product was labeled as Al-12Si@$Al(OH)_3$(H) abbreviated to A17H3, meanwhile, the Al-12Si@$Al(OH)_3$ synthesized by water bath method for 3h was labeled as Al-12Si@$Al(OH)_3$(W) abbreviated to A17W3. The experimental parameters, i.e., reaction time, silicon content and Al-Si particle diameter, were changed to investigate the influence of different parameters on precursor microstructure.

Table 1
Parameters of Al-Si powders

Sample	Si content / at. %	Mean size / μm
Al-12Si(A17)	12	75
Al-20Si(A23)	20	38
Al-20Si(A27)	20	75
Al-30Si(A37)	30	75

The morphology of as-prepared core-shell composite was observed using a scanning electron microscope (SEM, JEOL JSM-6700F, Japan). X-ray diffraction (XRD) analysis was carried out using the Rigaku D/MAX-2500 X-ray diffractometer (Japan) with a scan rate of 10 °/min. The Fourier transform infrared (FTIR) spectroscopy was conducted using a Nicolet-5700 instrument. The pore structure and BET surface area were tested at 77 K via N_2 adsorption/desorption isotherms.

Results And Discussion

Analysis of samples

Figure. 1 presents the XRD patterns of various precursors prepared by the water bath and hydrothermal methods. The characteristic peaks of Al and Si can be clearly observed, however, a weak peak of the bayerite phase ($Al(OH)_3$, PDF# 20 – 0011) was observed in the XRD pattern of A17W6, which is consistent with the previous reports that the bayerite is formed by the reaction of Al with water [25]. The characteristic peaks of $Al(OH)_3$ phase in Figure. 1(c) and 1(d) were too weak and could not be observed in the XRD pattern. To further illustrate the existence of bayerite phase in hydrothermally-prepared precursors, the FTIR spectrum of A17H6 is shown in Figure. 2. The strong peak at 3435 cm^{-1} illustrates the existence of $Al(OH)_3$. Moreover, Al-O stretching vibrations are confirmed by the presence of peaks at 734 and 611 cm^{-1}, confirming the existence of $Al(OH)_3$[25]. It has been reported that Si is essential to form boehmite [19], i.e., the $Al(OH)_3$ is successfully formed in all precursors.

Figure. 3 presents SEM images of A27 prepared using different methods and times. It is objected that the thickness of nanosheets prepared by the water bath method is thinner than the hydrothermal method. It is perceived that the growth of nanosheets on the surface of Al-Si@$Al(OH)_3$(W) is abnormal and abundant impurities appear around the core-shell structure, decreasing the active sites and compromising the catalytic performance. Compared with the water bath method, the hydrothermal method is a better way to prepare pure Al-Si@$Al(OH)_3$. It is noteworthy that the increase in time only affects the thickness of nanosheets and we can decrease hydrothermal time to obtain equally distributed core-shell structures, shortening the preparation cycle.

As shown in Figure. 4, Al-Si@$Al(OH)_3$ can be synthesized using Al-Si powder with different amounts of Si. The thickness distribution of A27H6 is more concentrated than others, showing the influence of Si morphology on thickness uniformity of $Al(OH)_3$ nano-flakes.

To further investigate the influence of Al-Si particle size, two different grain sizes were utilized to form Al-20Si@$Al(OH)_3$(H). It is observed that there is a little distinction in morphology, as shown in Figure. 5(a-b). As the particle size of Al-Si powder influenced the Si morphology, the density of primary Si on the surface of Al-Si particles increased with the decrease of mean particle size. It can be concluded that the particle size renders a negligible influence on the structure of $Al(OH)_3$ nano-flakes. Figure. 6(a) presents the adsorption/desorption isotherms of A27H6, which belong to type-Ⅳ of IUPAC and indicate the presence of meso-pores. The specific surface area is found to be 19.5573 m^2/g, which indicates that the nano-flakes increased the specific surface area of Al-Si particles. The pore diameter of A27H6 is mainly distributed below 25 nm, as shown in Figure. 6(b).

Impact of silicon morphology

In order to reveal the growth mechanism during the initial stage, the ground and polished Al-20Si alloy was treated with deionized water at 80 ℃ for 30 minutes and morphological changes were observed, as

shown in Figure. 7. Overall, the distribution of nano-flakes was mainly focused on the interphase between Si phase and Al matrix, which indicates that the nucleation of $Al(OH)_3$ mainly occurs at the Al/Si interphase and the nanosheets completely cover the surface of Al-Si particle with the increase of reaction time. In addition, more nanosheets were observed on the surface of eutectic Si than the primary Si phase, which indicates the influence of Si area on $Al(OH)_3$ deposition.

Conclusion

In summary, the influence of Si content and Al/Si particle size on the morphology and thickness of $Al(OH)_3$ nanosheets has been systematically investigated. The main conclusions can be given as:

1. The comparison of microstructure between hydrothermal and water bath methods revealed that the hydrothermal method is a better way to prepare Al-Si@$Al(OH)_3$ nanosheets than the water bath method. Overall, the reaction time rendered a little effect on the structure of Al-Si@$Al(OH)_3$ nanosheets.

2. The SEM images and pore size analysis demonstrated that the average thickness of nano-flakes decreased with the increase of Si content. Moreover, the distribution density of $Al(OH)_3$ nanosheets remained constant when the mean particle size of Al-Si exceeded 38 μm.
3. The nucleation site of $Al(OH)_3$ nano-flaky was on interface between silicon and aluminum matrix in initial stage. Relative to the area of eutectic Si and Al matrix, the area of primary Si is finally covered by $Al(OH)_3$ nanosheets.

These results demonstrate that the preparation time of Al-Si@Al_2O_3 can be effectively reduced by regulating Si content and average particle size of Al-Si alloy. The current study offers an efficient strategy to synthesize Al-Si@Al_2O_3 core-shell structure for a wide array of applications.

Declarations

Acknowledgements

We thank the support from Science and Technology Project of State Grid Corporation of China (SGZJ0000KXJS1900221) and the National Natural Science Foundation of China (Grant No. 51672145).

Author contributions statement

Y.L. wrote the initial drafts of the work. All the authors contributed to the discussion. All authors read and approved the final manuscript.

Competing interests

The authors declare no competing interests.

References

1. Singh, R. and Bhateria, R. Core–shell nanostructures: a simplest two-component system with enhanced properties and multiple applications. *Environ. Geochem. Health* 10.1007/s10653-020-00766-1 (2020).
2. Chang, Y. C. and Lin, Y. W. MoS_2@SnO_2 core-shell sub-microspheres for high efficient visible-light photodegradation and photocatalytic hydrogen production. *Mater. Res. Bull.* **129,** 110912 (2020).
3. Zou, Q. C., Jie, J. C., Shen, Z. F., Han, N. and Li, T. J. A new concept of Al-Si alloy with core-shell structure as phase change materials for thermal energy storage. *Mater. Lett.* **237,** 193-196 (2019).
4. Liu, X. M., Niu, C. G., Zhen, X. P., Wang, J. D. and Su, X. T. Novel approach for synthesis of boehmite nanostructures and their conversion to aluminum oxide nanostructures for remove Congo red. *J. Colloid Interface Sci.* **452,** 116-125 (2015).
5. Li, G. X., Wu, C., Dong, P., Ji, D. and Zhang, Y. F. Core–Shell HZSM-5@silicalite-1 composite: controllable synthesis and catalytic performance in alkylation of toluene with methanol. *Catal. Lett.* **150,** 1923-1931 (2020).
6. Yang, L. Q., et al. $Co_{5.47}$N/rGO@NF as a high-performance bifunctional catalyst for urea-assisted hydrogen evolution. *Catal. Lett.* **149,** 3111-3118 (2019).
7. Wang, Y., Hao, X., Wang, G. and Jin, Z. Rational Design of a Core–Shell-Shaped Flowerlike Mn0.05Cd0.95S@NiAl-LDH Structure for Efficient Hydrogen Evolution. *Catal. Lett.* **151,** 634-647 (2021).
8. Xie, C., et al. Effect of cores on photoluminescence of hybrid SiO_2-coated CdTe quantum dots. *J. Nanosci. Nanotechnol.* **20,** 5478-5485 (2020).
9. Yao, C. L. and Zhu, J. M. Synthesis, characterization and photocatalytic activity of Au/SiO_2@TiO_2 core-shell microspheres. *J. Braz. Chem. Soc.* **31,** 589-596 (2020).
10. Gandomi, F., Sobhani-Nasab, A., Pourmasoud, S., Eghbali-Arani, M. and Rahimi-Nasrabadi, M. Synthesis of novel Fe_3O_4@SiO_2@Er_2TiO_5 superparamagnetic core–shell and evaluation of their photocatalytic capacity. *J. Mater. Sci.: Mater. Electron.* **31,** 10553-10563 (2020).
11. Han, D. D., Xiao, N. R., Liu, B., Song, G. X. and Ding, J. One-pot synthesis of core/shell-structured NiS@onion-like carbon nanocapsule as a high-performance anode material for Lithium-ion batteries. *Mater. Lett.* **196,** 119-122 (2017).
12. Li, S. T., et al. Core-shell structured Co@CN nanocomposites as highly efficient dual function catalysts for reduction of toxic contaminants and hydrogen evolution reaction. *Nanotechnology* **31,** 065701 (2019).
13. Quan, F., et al. Cu/Ag core/shell particles via modified arc discharge method. *Int. J. Mater. Res.* **109,** 270-272 (2018).

14. Ren, Y. Y., et al. Pd@Pt core–shell nanoflowers as efficient catalyst toward methanol oxidation. *Catal. Lett.* **150,** 3415-3423 (2020).
15. Wang, Z. T. Cycloaddition of propargylic amines and CO_2 by Ni@Pd nanoclusters confined within metal–organic framework cavities in aqueous solution. *Catal. Lett.* **150,** 2352-2364 (2020).
16. Zhang, X. T., He, N., Liu, C. Y. and Guo, H. C. Pt–Cu alloy nanoparticles encapsulated in silicalite-1 molecular sieve: coke-resistant catalyst for alkane dehydrogenation. *Catal. Lett.* **149,** 974-984 (2019).
17. He, F., Sui, C., He, X. D. and Li, M. W. Comparison of structure and phase change characteristic of microencapsulated core/shell Al–Si alloy microparticles synthesized by two methods. *J. Sol-Gel Sci. Technol.* **76,** 1-10 (2015).
18. Daraio, D., et al. Using Discrete Element method (DEM) simulations to reveal the differences in the γ-Al_2O_3 to α-Al_2O_3 mechanically induced phase transformation between a planetary ball mill and an attritor mill. *Miner. Eng.* **155,** 106374 (2020).
19. Liu, G. G., et al. A facile method for in situ growing nano-flaky γ-Al_2O_3 on the surface of Al–Si alloy sphere. *J. Alloys Compd.* **647,** 18-23 (2015).
20. Dai, Y. N., et al. Preparation and catalytic application Al-Si@Al_2O_3 core-shell structured carrier. *Nonferrous Metals Science and Engineering* **7,** 42-48 (2016).
21. Hearn, W., Bogno, A. A., Spinelli, J., Valloton, J. and Henein, H. Microstructure Solidification Maps for Al-10 Wt Pct Si Alloys. *Metall. Mater. Trans. A* **50,** 1333-1345 (2019).
22. Cai, Z. Y., et al. Effect of solidification rate on the coarsening behavior of precipitate in rapidly solidified Al-Si alloy. *Prog. Nat. Sci.: Mater. Int.* **26,** 391-397 (2016).
23. Cai, Z. Y., et al. Improvement of deformation capacity of gas-atomized hypereutectic Al-Si alloy powder by annealing treatment. *Trans. Nonferrous Met. Soc. China* **28,** 1475-1483 (2018).
24. Cai, Z. Y., et al. Characterization of rapidly solidified al-27 si hypereutectic alloy: Effect of solidification condition. *J. Mater. Eng. Perform.* **24,** 1226-1236 (2015).
25. Godart, P., Fischman, J., Seto, K. and Hart, D. Hydrogen production from aluminum-water reactions subject to varied pressures and temperatures. *Int. J. Hydrogen Energy* **44,** 11448-11458 (2019).

Figures

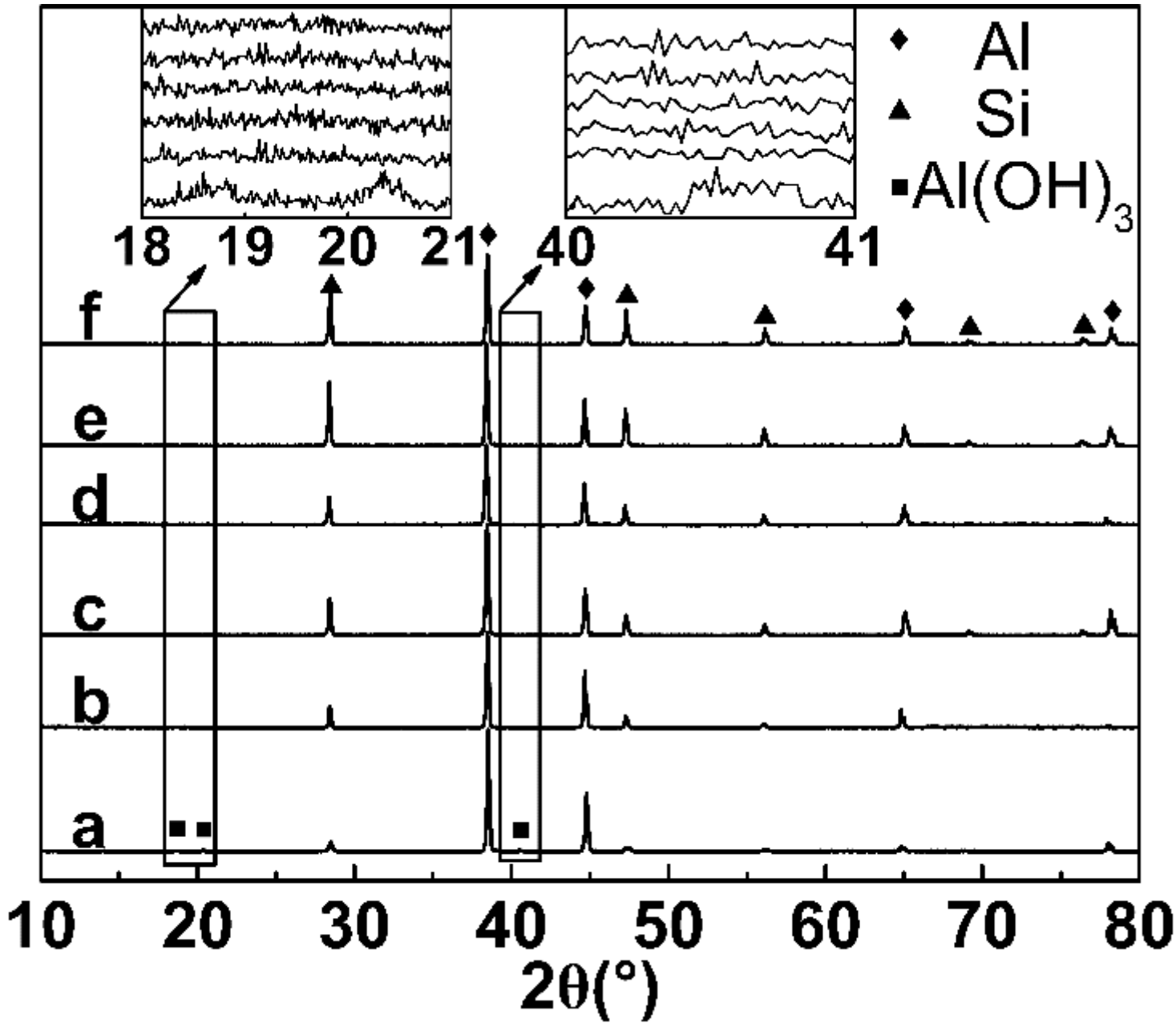

Figure 1

XRD patterns of precursors: (a)A17W6, (b)A17H6, (c)A27W6, (d)A27H6, (e)A37W6 and (f)A37H6.

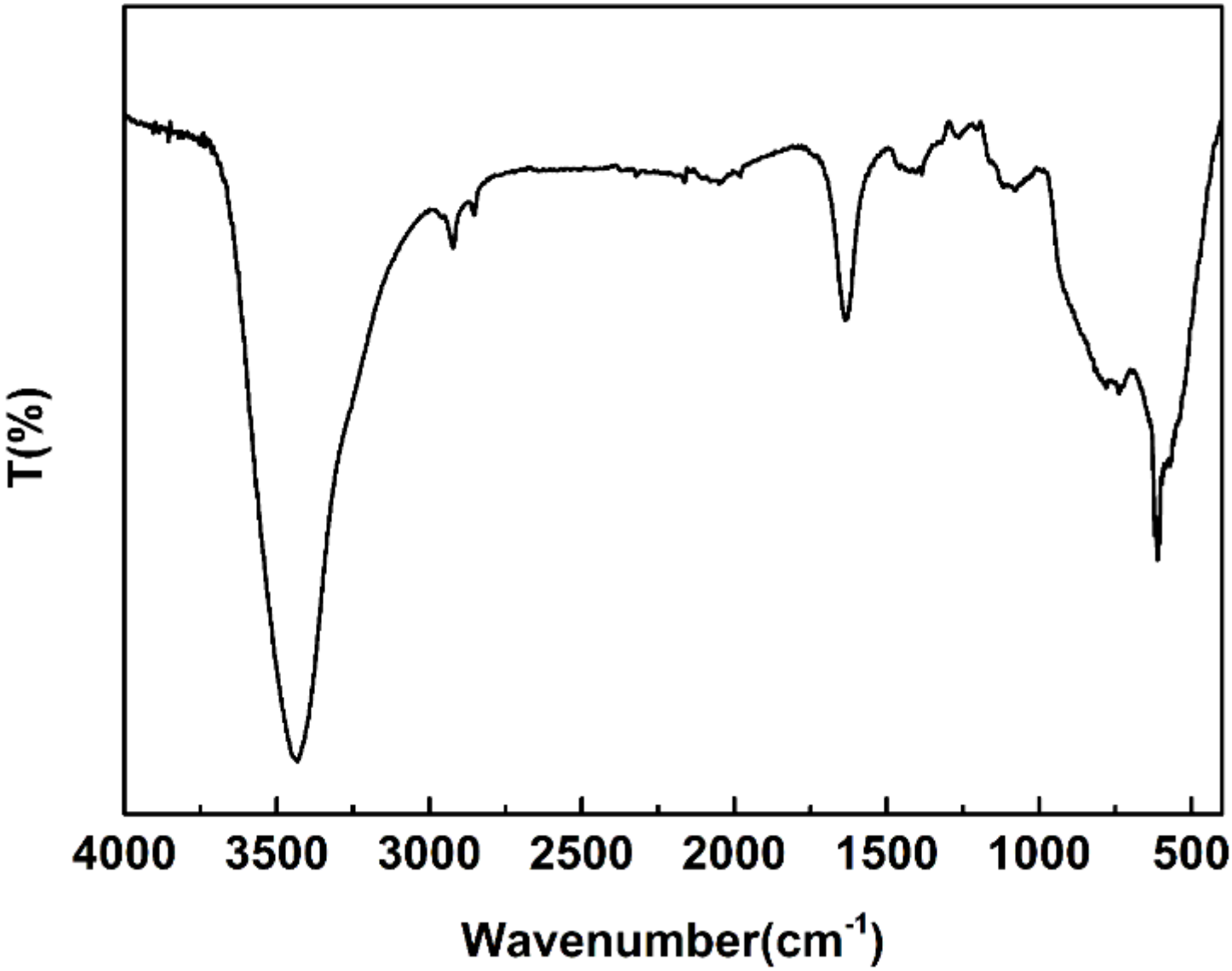

Figure 2

FTIR spectrum of A17H6.

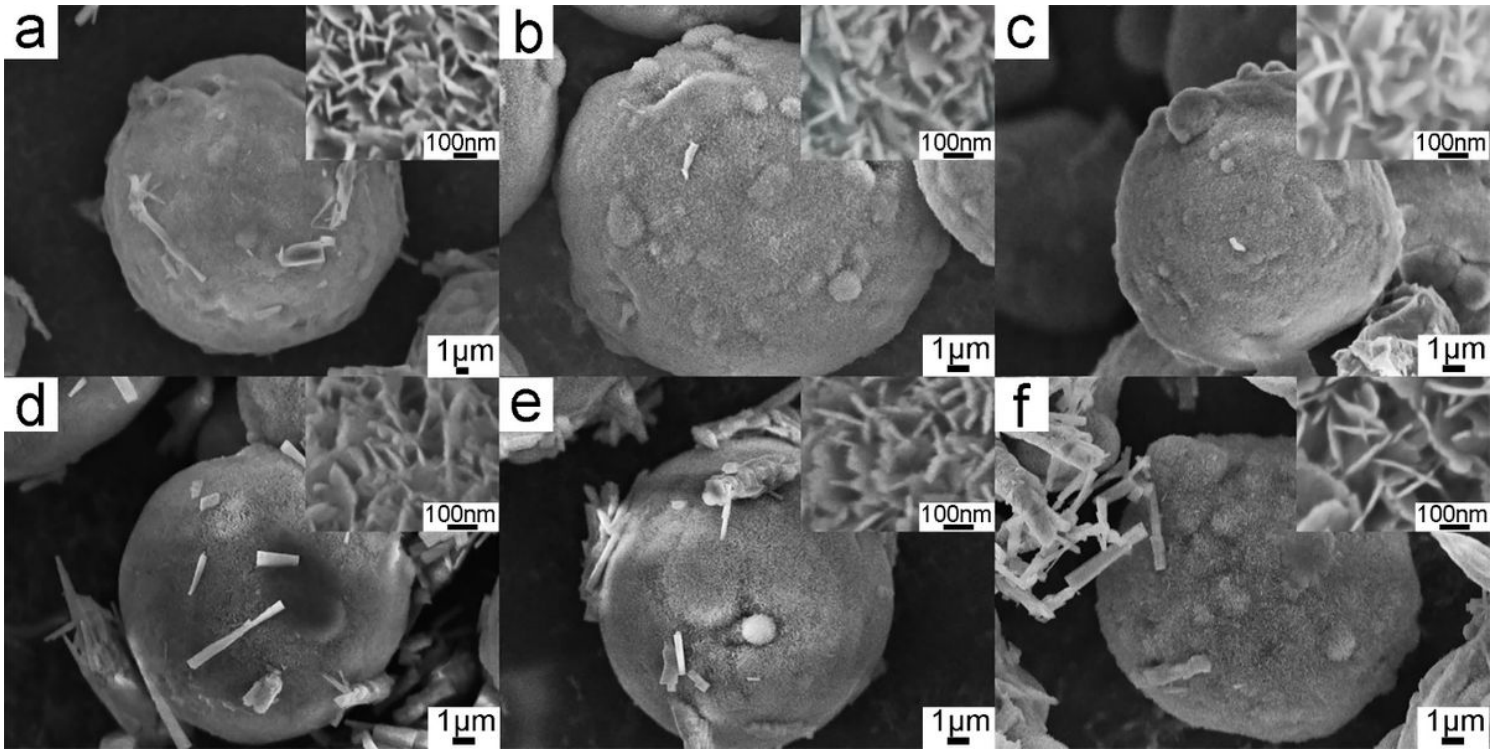

Figure 3

SEM images of precursors: (a)A27H3, (b)A27H6, (c)A27H9, (d)A27W3, (e)A27W6 and (f)A27W9.

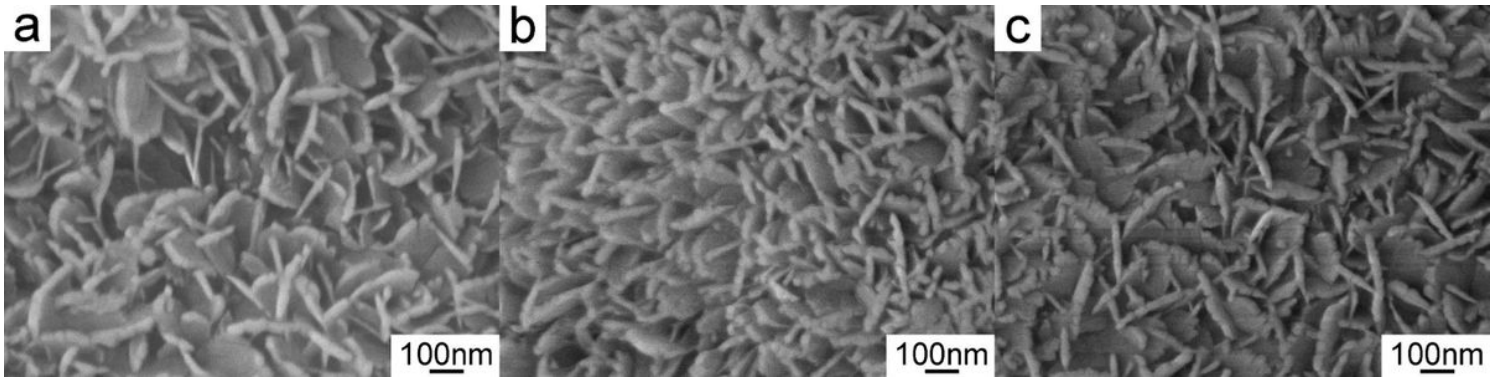

Figure 4

SEM images of (a)A17H6, (b)A27H6, and (c)A37H6.

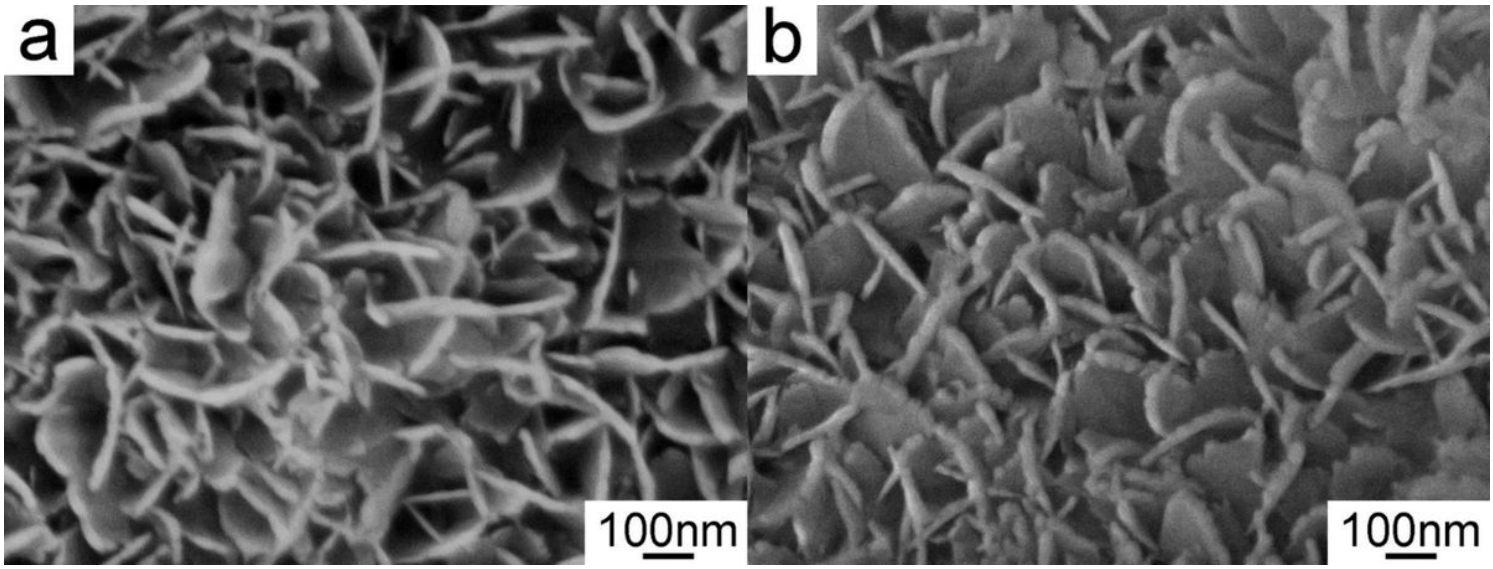

Figure 5

Surface morphologies of (a)A23H6 and (b)A27H6.

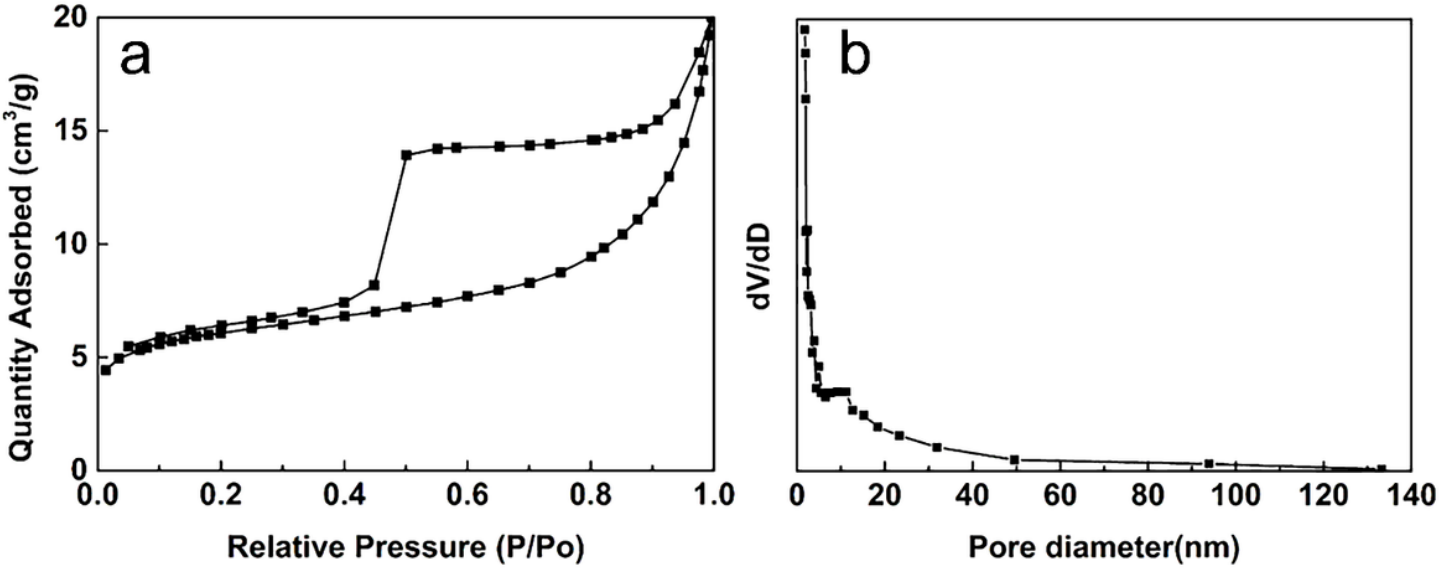

Figure 6

A27H6 about (a)adsorption/desorption isotherms and (b)pore size distribution.

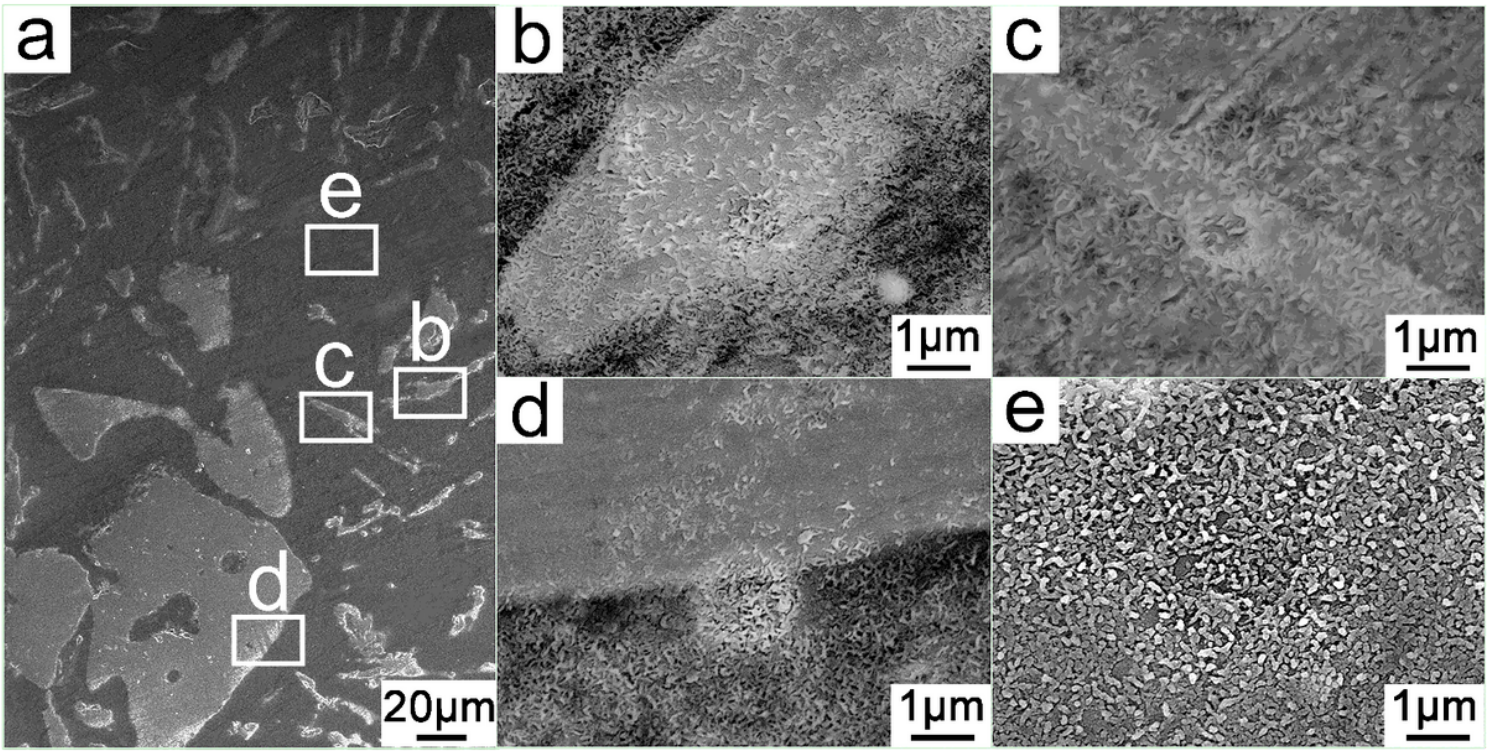

Figure 7

The morphology of Al-20Si@Al(OH)3(W):(a)Al-20Si, (b, c)eutectic silicon, (d)primary silicon, and (e)aluminum.